Effects of Structural Variations on the Cellular Response and Mechanical Properties of Biocompatible, Biodegradable, and Porous Smectic Liquid Crystal Elastomers

Anshul Sharma, Taizo Mori, Cory J. Mahnen, Heather R. Everson, Michelle T. Leslie, Alek d. Nielsen, Laurent Lussier, Chenhui Zhu, Christopher Malcuit, Torsten Hegmann, Jennifer A. McDonough, Ernest J. Freeman, LaShanda T. J. Korley, Robert J. Clements,* Elda Hegmann*

The authors report on series of side-chain smectic liquid crystal elastomer (LCE) cell scaffolds based on star block-copolymers featuring 3-arm, 4-arm, and 6-arm central nodes. A particular focus of these studies is placed on the mechanical properties of these LCEs and their impact on cell response. The introduction of diverse central nodes allows to alter and custom-modify the mechanical properties of LCE scaffolds to values on the same order of magnitude of various tissues of interest. In addition, it is continued to vary the position of the LC pendant group. The central node and the position of cholesterol pendants in the backbone of ε-CL blocks (alpha and gamma series) affect the mechanical properties as well as cell proliferation and particularly cell alignment. Cell directionality tests are presented demonstrating that several LCE scaffolds show cell attachment, proliferation, narrow orientational dispersion of cells, and highly anisotropic cell growth on the as-synthesized LCE materials.

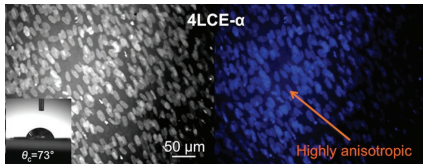

Dr. A. Sharma,[+] Dr. T. Mori,[++] C. J. Mahnen, A. d. Nielsen, Prof. T. Hegmann, Prof. E. Hegmann
Liquid Crystal Institute (LCI)
Chemical Physics Interdisciplinary Program (CPIP)
Kent State University
Kent, OH 44242-0001, USA
C. J. Mahnen, H. R. Everson, A. d. Nielsen, Prof. C. Malcuit, Prof. J. A. McDonough, Prof. E. J. Freeman, Prof. R. J. Clements, Prof. E. Hegmann
Department of Biological Sciences
Kent State University
Kent, OH 44242-0001, USA
E-mail: rclement@kent.edu; ehegmann@kent.edu
M. T. Leslie, Prof. L. T. J. Korley
Macromolecular Science and Engineering Department
Case Western Reserve University
Cleveland, OH 44106-7202, USA
L. Lussier, Prof. T. Hegmann, Prof. E. Hegmann
Department of Chemistry and Biochemistry
Kent State University
Kent, OH 44242-0001, USA
Dr. C. Zhu
Advanced Light Source
Lawrence Berkeley National Laboratory
Berkeley, CA 94720, USA

[+]Present address: Physics and Materials Science Research Unit, Université du Luxembourg, Campus Limpertsberg, 162a avenue de la Faïencerie, BS 1.15c, L-1511 Luxembourg

[++]Present address: World Premier International (WPI) Research Center for Materials, Nanoarchitectonics (MANA), National Institute for Materials Science (NIMS), 1-1 Namiki, Tsukuba 305-0044, Japan

DOI: 10.1002/mabi.201600278

1. Introduction

Synthetic and bioinspired cellular scaffolds can promote the development of the biophysical and biochemical environment of seeded cells called the extra cellular matrix (ECM). The ECM is a complex and dynamic system consisting of biomacromolecules that surround the cells and governs the cellular behavior including cell differentiation, proliferation, migration, viability, and other specific functions.[1,2] There are numerous examples of both natural and synthetic polymer systems that have been used as cell scaffolds.[3–7] Synthetic biodegradable polymers based on poly(ε-caprolactone), poly(lactic acid), poly(glycolide), poly(*p*-dioxanone), poly(carbonates), and poly(α-amino acids) as well as copolymers made of these building blocks have been explored to create cell scaffolds for applications such as implants, stents, sutures, in drug delivery, wound dressings, as injectable ECMs, and in multiple other clinical applications.[8–16] Key advantages of these materials are the possibilities to easily tailor their chemical and mechanical properties as well as biodegradation simply by introducing small changes in their chemical compositions.[4,6,17] However, the structural space for these materials is massive and further modifications, for example by introducing entirely new physical properties, could result in tunable and new, unexpected cell–scaffold interactions. There are several examples in the literature that have shown that the physical properties of polymer scaffolds such as elasticity,[18,19] anisotropy,[20–22] geometry,[23] 3D, and other physical features[10,24–28] of scaffolds play a crucial role in cell behavior, promotion of ECM, cell–ECM interaction, and tissue regeneration.

Liquid crystals (LCs) have intrinsic anisotropic properties making them ideal candidates to be incorporated within cell scaffold systems.[29] In this respect, especially liquid crystal elastomers (LCEs) present a unique example of a combination between LC properties and elastic polymer response.[30] LCEs are a special class of soft materials featuring orientational order, stimuli-responsive shape changes as well as elasticity. LCEs have found applications in photoresponsive devices, LC gels, as artificial muscles, and actuators.[31–35] Recent research has shown that the orientational ordering of nematic LCs can influence cell attachment and proliferation.[29,36] Previous work from our group has shown that both nematic and smectic biodegradable, biocompatible and porous LCEs with "Swiss-cheese" like morphology,[37] 3D channel or foam-like[38] as well as globular morphology[39,40] are viable candidates for active cell scaffolds that support the attachment and proliferation of cells, further expanding possibilities toward tissue regeneration.[37–40]

As a proof-of-concept for the suitability of LCEs as viable cell scaffolds, we recently introduced smectic cholesterol-functionalized P-ε-CL/(D,L)-LA cross-linked star block-copolymers, where the position of the cholesterol pendant group was varied (α or γ to the CL carbonyl group). These LCE scaffolds were intrinsically porous exhibiting the above-mentioned "Swiss-cheese" morphology, permitting both the attachment and proliferation of various cell lines such as neuroblastomas and skeletal muscle cells (myoblasts). While the position of the LC pendant group (α or γ to the carbonyl group along the polymer backbone) had some effects on the mechanical properties of these LCE cell scaffolds, a much larger effect would be expected from structural modification related to connectivity and the density of cross-linking.

To do so, we here present the synthesis and characterization of new series of smectic LCE cell scaffolds based on cross-linked star block copolymers (SBC) with 3-arm, 4-arm, and 6-arm central nodes, adjusting simultaneously the connectivity and the degree of cross-linking between individual polymer strands. These architectural handles should allow us to alter and custom-modify the mechanical properties of these LCEs by one simple synthetic variation to values closely matching those of various tissues of interest,[41] along with promoting superior and stimuli-responsive surface properties for cell attachment. Cholesterol was again selected as the LC pendant in our system due to both its mesogenic nature bioactive role in cell membranes and occurrence in biological tissues.[42,43] LC polymers containing cholesterol have been studied as biodegradable polymers to study cell interactions and drug delivery.[44,45] The data presented here will focus particularly on the surface and mechanical properties and their impact on cell response of these LCEs with 3-arm, 4-arm, and 6-arm networks with variable elasticity. In addition, we continued to vary the position of the LC pendant group. To prepare 3-arm-LCEs-α/γ, 4-arm-LCEs-α/γ, and 6-arm-LCEs-α/γ, glycerol (3-arm), pentaerythritol (4-arm), and dipentaerythritol (6-arm) were used as central nodes, respectively (see Scheme 1 for structures and synthesis). The obtained elastomers (3LCE-α, 3LCE-γ, 4LCE-α, 4LCE-γ, 6LCE-α, and 6LCE-γ) were fully characterized and then tested with respect to their mechanical properties, biocompatibility and cell viability in cell cultures using mouse skeletal myoblasts (C2C12) and human dermal fibroblast (hDF) cell lines.

2. Experimental Section

2.1. Materials

All air sensitive manipulations were carried out under nitrogen gas. ε-caprolactone (ε-CL, from Alpha Aesar) was dried over calcium hydride and distilled under reduced pressure. Glycerol, cholesterol, pentaerythritol, dipentaerythritol, triethylamine, stannous 2-ethylhexanoate, chromium (VI) oxide, sodium sulfate, pyridinium chlorochromate, and sodium bicarbonate were

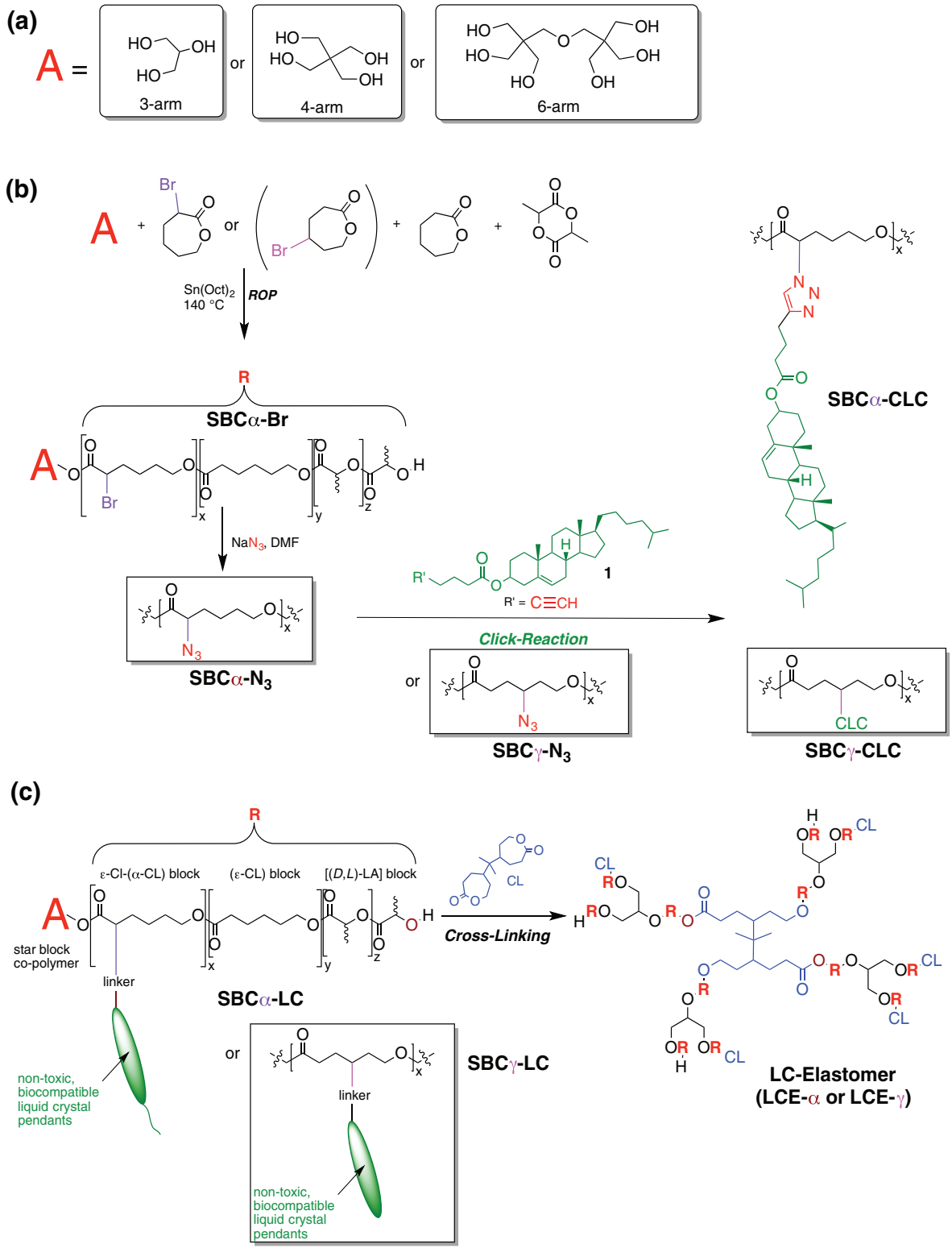

Scheme 1. a) Chemical structure of 3-arm, 4-arm, and 6-arm initiators (central nodes) and b) synthesis pathway to star block copolymer-cholesterol liquid crystal (SBCα-CLC) (showing a purple link) and SBCγ-CLC (showing a pink link). The ratio of all caprolactones to D,L-lactide is 1:1; the ratio between LC-modified and nonmodified caprolactone is 1:10. c) Crosslinking with bis-caprolactone (BCP) to obtain a 3-arm alpha (or gamma) positioned LCE. For abbreviations of LCEs see Table 1.

Table 1. Names of elastomers samples studied.

Sample	Elastomer name[a)]
Unmodified elastomers	3E
	4E
	6E
α-series	3LCE-α
	4LCE-α
	6LCE-α
γ-series	3LCE-γ
	4LCE-γ
	6LCE-γ

[a)]Arabic numbers in front of elastomer name (3, 4, or 6) indicate the number of elastomer arms of the central node (initiator). Alpha (α) or gamma (γ) series indicate position of the LC triazole moiety with respect to the caprolactone carbonyl group.

used as received (Sigma-Aldrich). Sodium thiosulfate purchased from Fisher Scientific was used as received. 3-Chloroperbenzoic acid (*m*-CPBA, from Sigma-Aldrich) was dissolved in diethyl ether and this ether solution was washed with a buffer solution (prepared from 1.28 g sodium phosphate monobasic monohydrate and 8.24 g sodium phosphate dibasic heptahydrate in 800 mL distilled water at pH = 7.4). All solvents used for the synthesis and purification were EMD Millipore grade purified by a PureSolv solvent purification system (Innovative Technology Inc.). Dulbecco's modified Eagle medium (DMEM) with 4.5 g L^{-1} glucose and sodium pyruvate without L-glutamine and Dulbecco's phosphate buffered saline (PBS) without calcium and magnesium were purchased from Corning CellGrO. Penicillin streptomycin solution (Pen-Strep) was purchased from Thermo Scientific. Fetal bovine serum (FBS) and trypsin were purchased from HyClone. Formaldehyde solution for molecular biology, 36.5%–38% in H_2O was purchased from SIGMA Life Science. CyQuant Cell Perforation Assay Kit, 4′,6-diamidino-2-phenylindole (DAPI), UltraPure Agarose were purchased from Invitrogen. Reagent Alcohol 200 proof ACS Grade (Denatured Ethanol) was purchased from VWR. Mouse skeletal cell line (C2C12) and human primary dermal fibroblast normal cells (hDFs) were purchased from American Type Culture Collection.

2.2. Methods

2.2.1. ^{1}H Nuclear Magnetic Resonance (NMR), ^{13}C NMR, and Fourier Transform Infrared Spectroscopy (FT-IR)

Proton and carbon NMR spectra of copolymers were recorded in $CDCl_3$ at room temperature on a Bruker DMX 400 MHz instrument and referenced internally to residual peaks at 7.26 (^{1}H). Infrared spectroscopy of polymers was recorded using a Bruker Vector 33 spectrometer equipped with attenuated total reflection (ATR) mode.

2.2.2. Thermal Properties of SBCs and Final Elastomers

Differential scanning calorimetry (DSC) was used to obtain glass transition temperatures of the star block-copolymers and LC elastomers. Thermal phase transitions were recorded with a Thermal Perkin Elmer Pyris1 analyzer with a scanning rate of 10 °C min^{-1} from −70 to 250 °C under a nitrogen atmosphere. Thermal degradation studies were carried out with Hi-Res thermal gravimetric analysis (TGA)-2950 thermal analyzer under nitrogen atmosphere with ramp of 10 °C min^{-1}.

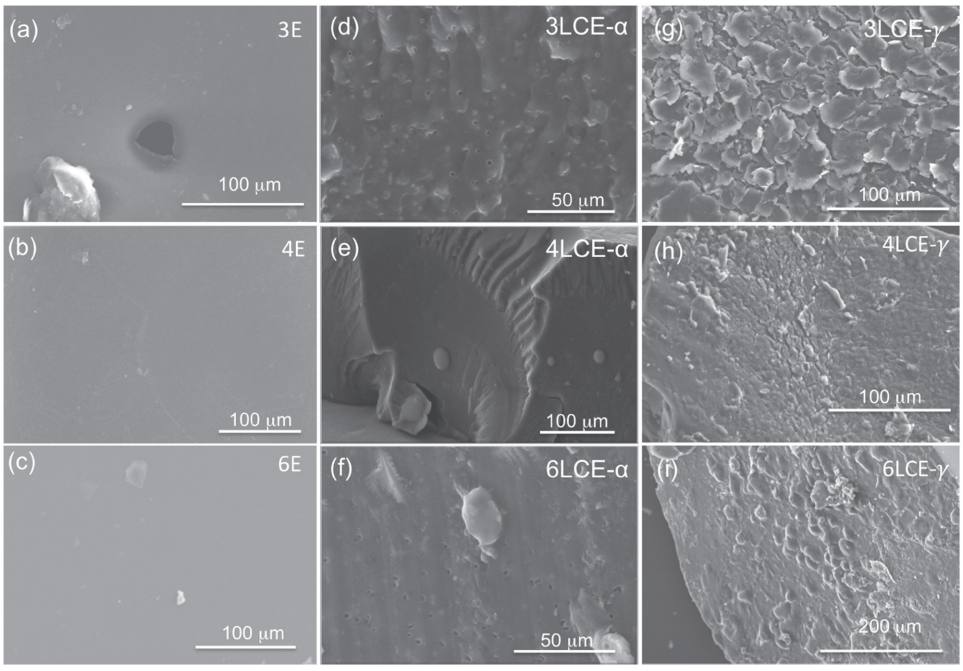

Figure 1. SEM images showing the internal morphology of a) 3E, b) 4E, c) 6E films, d) 3LCE-α, e) 4LCE-α, f) 6LCE-α, g) 3LCE-γ, h) 4LCE-γ, and i) 6LCE-γ.

2.2.3. Morphology of Elastomers

Scanning electron microscopy (SEM) was used to visualize and study elastomer morphology. All samples were freeze fractured (to study the internal morphology) and then gold coated (700 Å) using a sputter coater (Hummer VI-A, Anatech Ltd.) at 10 mA DC for 3 min and images were acquired using a Hitachi S-2600N SEM.

2.2.4. Small-Angle X-Ray Diffraction (SAXD) of Elastomers

SAXD was used to determine liquid crystalline phases of liquid crystal modified copolymers and elastomers (LCEs). SAXD data were data collected at the X-ray Operations and Research Beamline 12-ID-B at the Advanced Photon Source, Argonne National Laboratory for unmodified elastomers. For γ-LCEs, SAXD data were collected at beamline 7.3.3 of the Advanced Light Source (ALS) at Berkeley.[46] Samples at the ALS were mounted on a TST350 Linkam tensile stage.

2.2.5. Optical Microscopy

Polarized optical microscopy (POM) was performed using an Olympus BX53 polarizing microscope (20×) equipped with a Linkam LTS420 heating/cooling stage. All samples were initially heated to the isotropic liquid phase and then cooled to observe the temperature range at a rate of 0.1 °C. Fluorescence confocal microscopy was carried out using an Olympus FV1000 equipped with three laser lines and ImageJ was used for image analysis/processing.[47] Fluorescence for cell proliferation was measured using a Molecular Devices M4 SpectroMax Multi-Mode Microplate Reader.

2.2.6. Mechanical Testing of Elastomers

Uniaxial tensile testing (Zwick/Roell Z0.5, 100 N load cell) was performed under ambient conditions at a strain rate of 40% min^{-1}

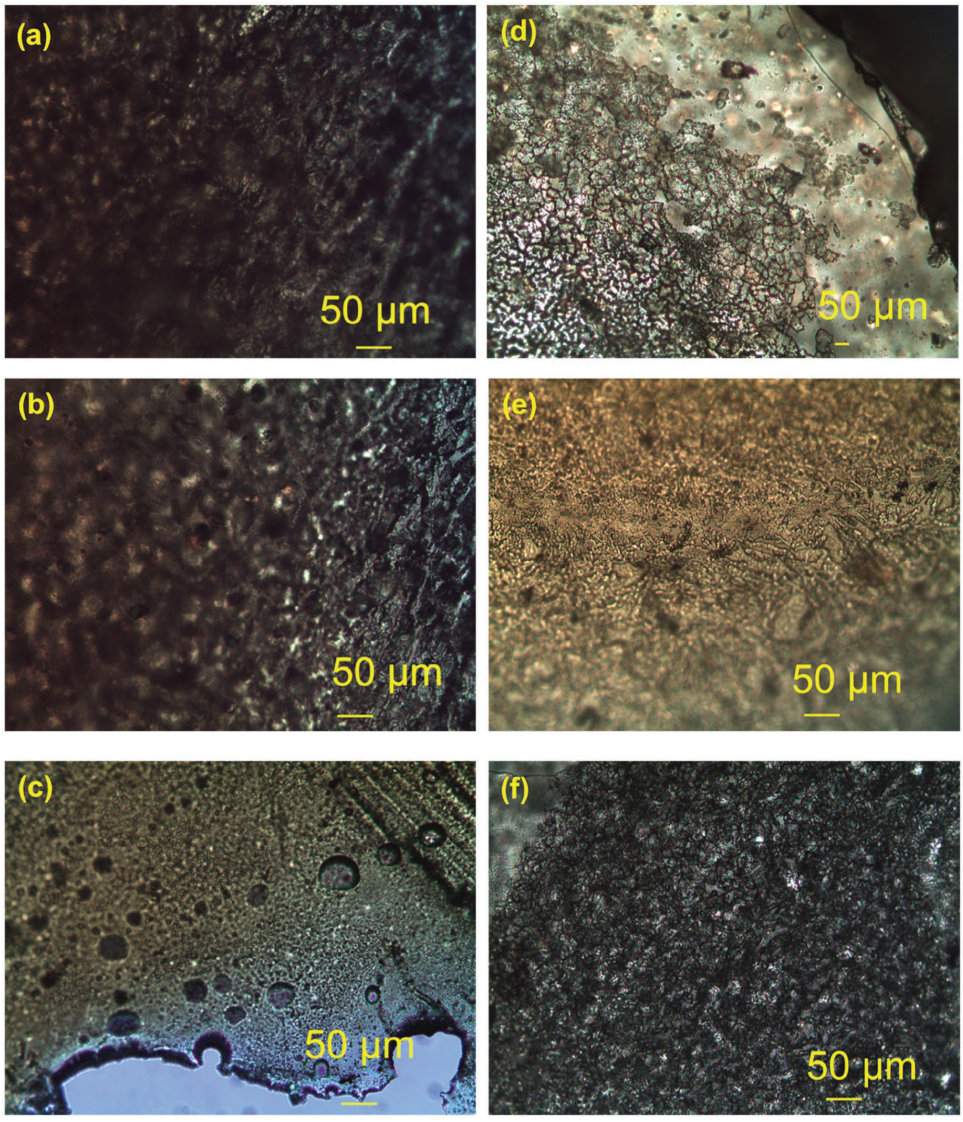

Figure 2. POM images of LCEs between untreated glass slides on cooling from the isotropic liquid phase (90° crossed polarizers) of a) 3LCE-α (at 53.4 °C), b) 4LCE-α (at 75.0 °C), c) 6LCE-α (at 31.7 °C), d) 3LCE-γ (at 30.7 °C), e) 4LCE-γ (at 49.9 °C), and f) 6LCE-γ (at 41.5 °C).

on solvent-cast elastomeric films. A modified version of ASTM D1708 was utilized for testing with the dimensions scaled down by a factor of two due to limited sample quantity. Five tensile samples per elastomer were examined for mechanical response; each sample was held between Mylar sheets during cutting to relieve stress concentrations along the sample edges. The elastic modulus (E) was determined from the slope of the stress–strain curve between 0.10% and 0.35% strain.

2.2.7. Contact Angle Measurements

Static water contact angle (WCA) measurements were completed using a CAM 200 optical contact angle meter (KSV Instruments LTD). The WCA value was acquired by forming single water drop at the tip of the syringe, bringing the sample up to the drop, and pulling it away on the sample. The drop was then allowed to achieve equilibrium on the sample by waiting two minutes. Contact angles were collected and averaged from two separate drops per sample using KSV CAM 2008 software.

2.2.8. Cell Cultures

Elastomers were seeded with mouse skeletal C2C12 myoblast cells or hDFs cells and cultured using standard sterile techniques. Growth medium for C2C12 contained 90% DMEM, supplemented with 10% FBS and 1% Pen-Strep. The elastomers were cut by using 8 mm diameter tissue punch and separated into four pieces with equal size. Prior to cell seeding, the elastomers were washed with 70% ethanol, UV irradiated for 10 min, and then washed by 70% ethanol again, rinsed twice with sterile water and PBS. Elastomers were pinned onto a 2% agarose with DMEM substrate to prevent cell adhesion to the petri dish culture surface in 24-well culture plates. Approximately 1.5×10^4 C2C12 cells (passages 8–12) suspended in growth 100 μL media were seeded onto each of the elastomers. The elastomers along with the cells were incubated at 37 °C with 5% CO_2, in a humidified chamber, for about 2 h to promote cell adhesion followed by addition of 0.5 mL growth media. Media was changed every other day after washing by 0.5 mL PBS. After 3, 5, 8, and 15 d, cells were fixed with 4% paraformaldehyde in PBS for 15 min, rinsed twice with PBS for 5 min. The fixed samples were stained with 0.1% DAPI with PBS for 10 min and rinsed twice with PBS for 5 min for fluorescence confocal microscopy analysis. Several images from the fluorescence confocal microscopy were sequentially taken and stacked into a 3D composite image using ImageJ. Image stacks were sequentially acquired using a fluorescence confocal microscope and spanned the sample thickness. 3D composite images were generated from the data and data analyzed using ImageJ. Similar protocols were followed for the hDF cultures.

2.2.9. Cell Proliferation and Cytotoxicity Assays

Viability and proliferation of C2C12 skeletal myoblasts of the elastomer scaffolding were assessed in a complimentary fashion using the CyQuant cell proliferation assay. For the CyQuant cell proliferation assay the elastomers were cut into equivalent size square pieces of 5 mm × 5 mm × 1 mm and quart circle pieces of 8 mm diameter, respectively. The elastomer pieces were sterilized

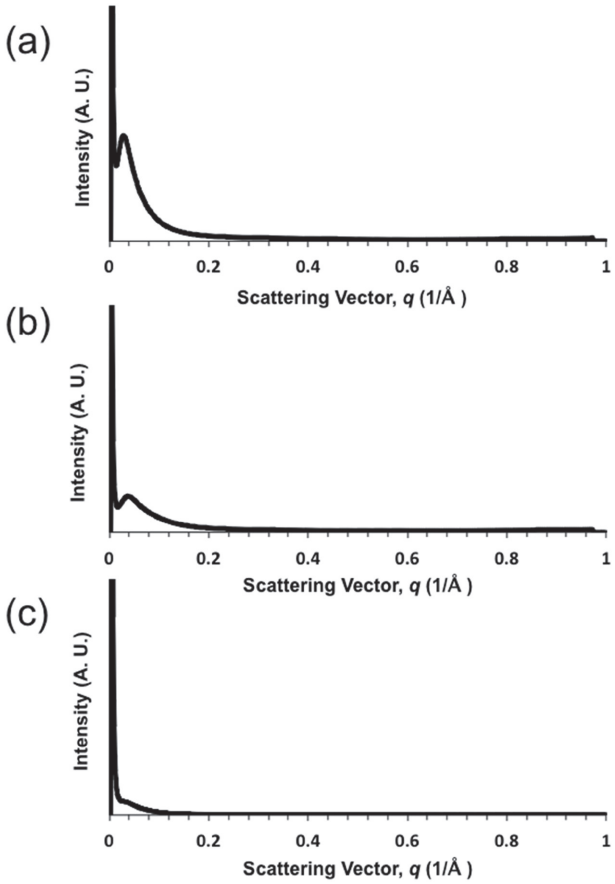

Figure 3. Azimuthally averaged intensity data of the scattering vector (q in $Å^{-1}$) versus intensity of 2D SAXD pattern with corresponding X-ray diffraction pattern of a) 3E, b) 4E, and c) 6E.

and seeded with 1.5×10^4 C2C12 or hDF cells, cultured for 15 d by the same method as described in the previous section (2.2.8). For the CyQuant cell proliferation assay, individual samples were removed at five time points (days 3, 5, and 8 for C2C12 as well as 6, 8, and 12 for hDF) and immediately frozen at −80 °C. At the completion of the culture period, the frozen elastomer/cell constructs were thawed and the cellular content was assessed using the CyQuant reagent according to the manufacturers recommended instructions, and fluorescence intensity was measured with excitation at 480 nm and emission at 520 nm.

2.2.10. Cell Imaging and Orientation Analysis

Confocal data were analyzed using ImageJ including the alignment and orientation of hDF cell nuclei where raw data were converted to grayscale, and the hDF nuclei were traced by stylus pen on Power Point. Next, the images were binarized and skeletonized for directionally analysis on ImageJ. In this calculation, the order parameter becomes better with increasing number of elongated cells, but the parameter is not dependent on the width of the cells. Specifications of the Directionality (Fiji) plug-in were followed as described by the method developed by Jean-Yves Tinevez.[47]

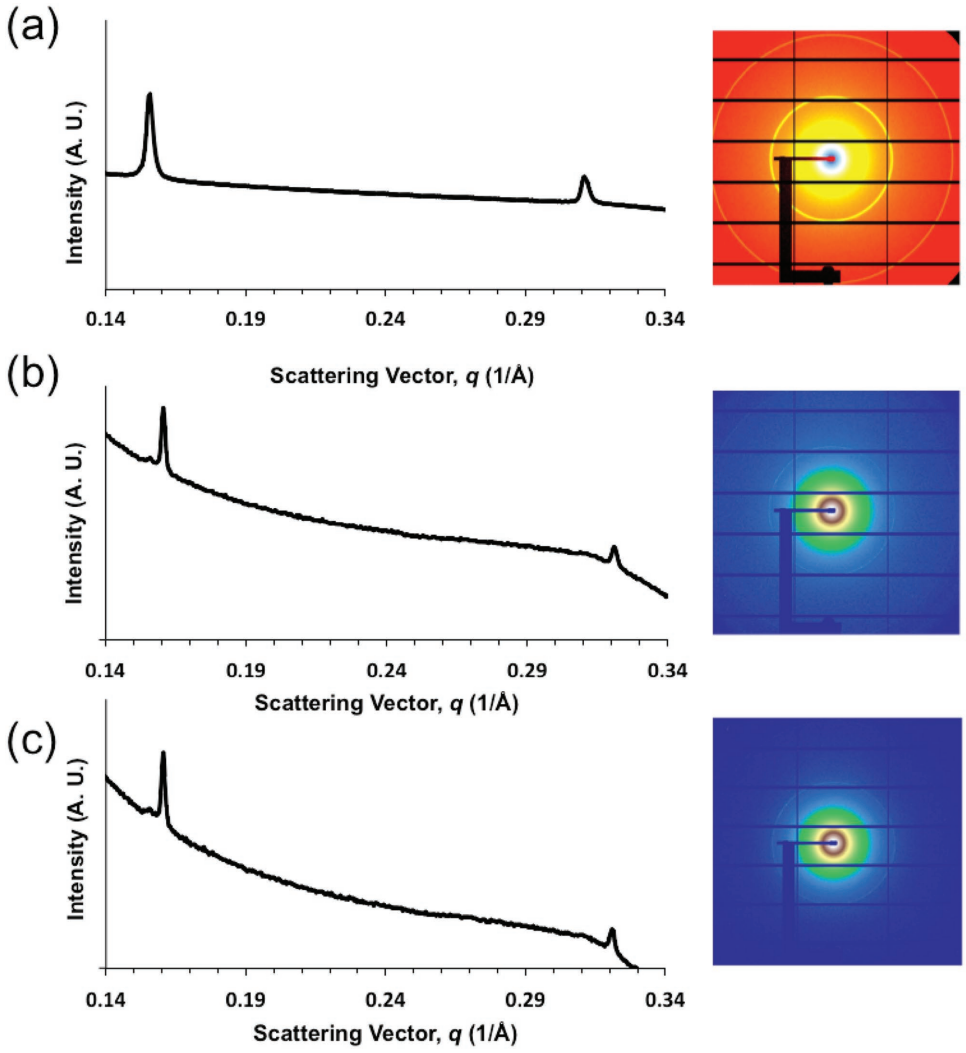

Figure 4. Azimuthally averaged intensity data of the scattering vector (q in Å^{-1}) versus intensity of 2D SAXD pattern with corresponding X-ray diffraction pattern of a) 3LCE-γ, b) 4LCE-γ, and c) 6LCE-γ.

2.3. Synthesis

For detailed synthesis and characterization data of reaction intermediates, monomers, copolymers, see the Supporting Information.

2.3.1. Liquid Crystal Elastomer Synthesis

Elastomers were prepared using a modified, previously reported method.[37,48] For the synthesis of 3LCE-α, LC-modified polymer (3-SBC$_1$-CLC), ε-caprolactone (ε-CL), and cross-linker 2,2-bis(1-caprolactone-4-yl) propane (BCP) at a ratio of 3:1:1 were used. In a clean dried flask 3-SBC$_1$-CLC (10%) (3 g), ε-CL (0.99 g, 8.7 mmol), BCP (0.99 g, 3.68 mmol), and 3 mL of dichloromethane were added, vortexed, and then heated in oven at 140 °C until the BCP was dissolved. Then, tin(II) 2-ethylhexanoate (90 µL, 0.28 mmol) as catalyst was added and contents were again mixed using vortex to obtain a homogeneous solution. Thus obtained mixture was poured over silanized glass substrates and kept at 140 °C for 24 h in a vacuum oven for cross-linking. The resulting elastomer was then removed and was washed with 70% ethanol solution and dried at 45 °C.

All other elastomer films (3LCE-γ, 4LCE-α, 4LCE-γ, 6LCE-α, and 6LCE-γ) were prepared following the exact same procedure, but replacing glycerol for pentaerythritol and dipentaerythritol to prepare the 4- and 6-arm LCEs, respectively. For comparison the authors also synthesized unmodified elastomers (using only ε-CL, eliminating the use of LC-modified CL). These are henceforth referred to as 3E (three-unmodified elastomer), 4E (four-unmodified elastomer) and 6E (six-unmodified elastomer). Table 1 shows a listing of all elastomers investigated in this study.

3. Results and Discussions

3.1. Synthesis and Chemical Characterization of Polymers and LCEs

The synthetic pathway pursued for the LC modified polymers is shown in Scheme 1. In a random ring opening polymerization ε-caprolactone (ε-CL), α-bromo-ε-caprolactone

Table 2. Measured scattering vectors (q in Å^{-1}) with respective Miller indices and calculated d spacing in nm.

Elastomer	$q_{(hkl)}$ [Å^{-1}]	d [nm]
3LCE-γ	$q_{(001)} = 0.155$	4.04
	$q_{(002)} = 0.31$	2.03
4LCE-γ	$q_{(001)} = 0.16$	3.94
	$q_{(002)} = 0.32$	1.98
6LCE-γ	$q_{(001)} = 0.153$	3.98
	$q_{(002)} = 0.316$	1.98

(α-Br-ε-CL), (D,L)-lactide (D,L-LA), and glycerol as 3-arm central node were polymerized using tin(II) 2-ethylhexanoate as a catalyst to obtain 3-arm star block-copolymer (3-SBCα-Br). Then, in subsequent steps the bromo (—Br) group was substituted with azide (—N_3) to obtain 3-SBCα-N_3. Displacement of the bromo (—Br) by the azide (—N_3) was confirmed by the appearance of the 2099 cm^{-1} band in the ATR FT-IR spectrum (Figure S1, Supporting Information) and higher chemical shifts of specific protons in the ^{1}H NMR spectra. The chosen LC pendant, cholesterylhexynoate, was covalently attached to the star block-copolymer using alkyne-azide Huisgen's cycloadditon reaction ("click" reaction)[37,49] obtaining 3SBCα-CLC. The disappearance of the 2100 cm^{-1} band and the appearance of a new band at 3263 cm^{-1} in the FT-IR spectra confirmed success of reaction (Figure S1, Supporting Information). The formation of the triazole ring was also confirmed by the presence of a singlet observed at 7.30 ppm in ^{1}H NMR spectra (NMR data, see the Supporting Information). We also studied effect of placement of halogen group either at alpha (α-Br) or gamma (γ-Cl) position to the carbonyl on the functionalized ε-CL (3SBCα-CLC or 3SBCγ-CLC). Then, we studied the effect of replacing the central node in the copolymers with 4-arm (4SBC-α/γ) and 6-arm (6SBC-α/γ) central cores. All central nodes serve as both initiators and intrinsic cross-linkers. At each step, the modification of functional groups was carefully monitored using ^{1}H NMR and FT-IR spectroscopy. ^{1}H NMR, FT-IR (Figures S1–S6, Supporting Information), TGA (Figures S7–S10, Supporting Information), and DSC (Table S1, Supporting Information) were used to characterize all star-block-copolymers before crosslinking (3-SBC-α/γ, 4-SBC-α/γ, and 6-SBC-α/γ, 3-SBC-α/γ, 4-SBC-α/γ, and 6-SBC-α/γ). Thereafter, all SBCs (3-SBC-αCLC, 3-SBC$_2$-γCLC, 4-SBC$_1$-αCLC, 4-SBC$_2$-γCLC, 6-SBC$_1$-αCLC, and 6-SBC$_2$-γCLC) were cross-linked using BCP to obtained 3LCE-α, 3LCE-γ, 4LCE-α, 4LCE-γ, 6LCE-α, and 6LCE-γ, respectively. DSC data confirmed that all modified SBCs were semicrystalline in nature while LCEs were amorphous and exhibited glass transition temperatures well below physiological temperature (see Table S2, Supporting Information). The glass transition temperatures and decomposition temperatures for all 3/4/6-SBC-α/γ and 3/4/6-LCE-α/γ are summarized in Tables S1 and S2 (Supporting Information), respectively.

SEM images (Figure 1) were taken to determine the surface and internal morphology of the obtained final LCEs of the α-series, γ-series as well as the unmodified elastomers (3E, 4E, and 6E). All α-LCEs show a porous "Swiss-cheese" type morphology (Figure 1d,e), whereas the γ-LCEs display a more flaky-type morphology (Figure 1g–i). The unmodified elastomers in contrast showed a much smoother surface as well as bulk when compared to the

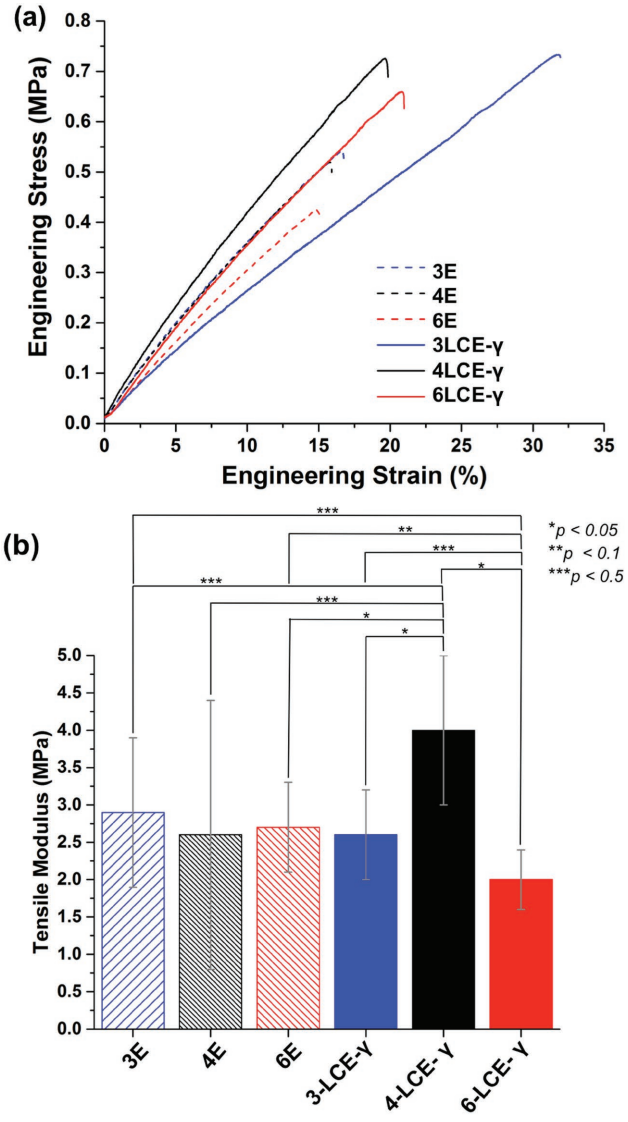

Figure 5. a) Stress–strain curve (representative curves determined by closest value to the average σ_M and ε_B) and b) elastic modulus data for γ-series LCEs and unmodified elastomers (3E, 4E, and 6E).

two LC-modified series (see Figure 2a–c). The difference in porosity and overall morphology could be explained by the presence and steric demand of the pendant cholesterol groups. With the LC pendants in the sterically more demanding α-position to the ε-CL carbonyl groups, less elastic but more porous structures are expected considering thermal expansion and contraction during cross-linking. The absence of LC pendant units leads to smooth materials for the nonmodified elastomers, and sterically more flexible LC pendants in the γ-position elastomers should lead to elastomers with lower porosity but higher elasticity.[37] We will see later that the mechanical properties of the α- and γ-series corroborate this to some extent.

3.2. Liquid Crystalline Properties and Morphological Characterization

The liquid crystalline properties of the LCEs were characterized using POM and SAXD. All the LCEs films (α and γ) were observed under temperature-controlled POM between plain, untreated glass slides (Figure 2). The textures were fairly nonspecific, and as frequently observed for LCEs, do not show characteristic textural patterns that would give any first insights into the possible LC phase formed. However, by gentle pressing, birefringent patterns (somewhat resembling the SEM morphological features) can clearly be seen in all images. The 2D SAXD patterns for the unmodified elastomers and the γ-LCEs are shown in Figures 3 and 4, respectively. Table 2 summarizes the X-ray diffraction data for the γ-LCEs. For the α-series, SAXD pattern for 3-LCE-α were reported earlier and provided clear evidence for the formation of a smectic-A phase with interdigitated cholesterol moieties.[37] 4-LCE-α and 6-LCE-α were too weak (less elastic, explained later in section 3.4) and the films broke during stretching to prepare thin films for SAXD measurement. However, they show similar textural features in POM and do likely form the same LC phase as all other LCEs reported here. The SAXD patterns for the γ-series each show two sharp scattering peaks in the mid-angle region

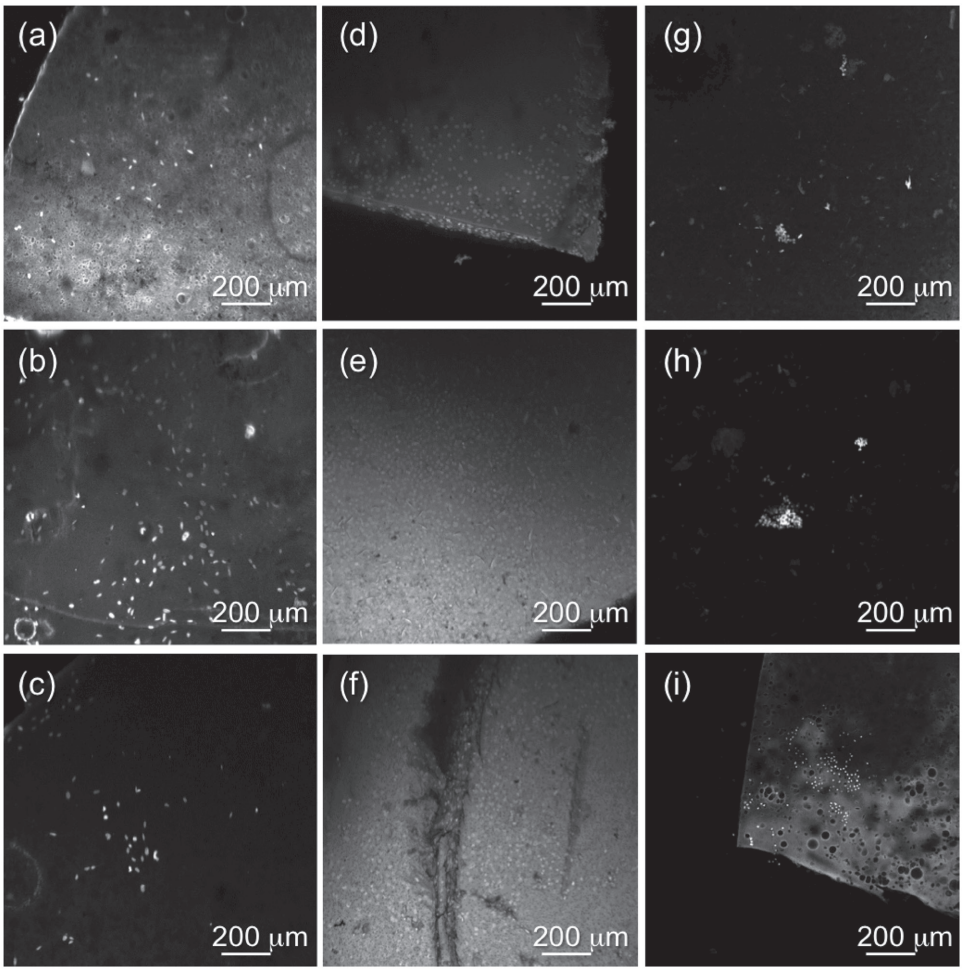

Figure 6. C2C12 skeletal myoblasts grown on the elastomers films for 8 d and nuclei stained with DAPI and data acquired using confocal microscopy a) 3E, b) 4E, c) 6E, d) 3LCE-α, e) 4LCE-α, f) 6LCE-α, g) 3LCE-γ, h) 4LCE-γ, and i) 6LCE-γ.

($q_1 \approx 0.15$–0.16 Å^{-1} and $q_2 \approx 0.32$ Å^{-1}) indicating ordered layer (i.e., smectic) structures (Figure 4). In addition, the q-values are rather similar to data previously reported by our group for the 3-arm α- and γ-position LCE materials.[37] In analogy, we assume that the values for 3-, 4-, and 6LCE-γ correspond to a nearly fully interdigitated smectic-A (SmA) phase type ordering. As shown in Figure 4 the SAXD patterns for the three unmodified elastomers show no sharps peaks in the same q-range (i.e., no peak with a maximum above 0.05 Å^{-1}), but broad scattering maxima at lower q-values (between 0.03 and 0.04 Å^{-1}) hinting at the amorphous nature of these elastomers.

3.3. Thermal Characterization of LCEs

TGA of all unmodified, α- and γ-elastomer series have higher decomposition temperatures (Figures S11–S15, Supporting Information) and are more stable that the more-volatile counterpart copolymers (Figure S7–S10, Supporting Information) which follows the pattern that we previously reported.[37] DSC data also corroborated our previous report[37] confirming all glass transition temperatures (T_g) values significantly below physiological temperatures. T_gs values increased after crosslinking and all elastomers appeared amorphous showing no presence of endothermic melting peaks (see Tables S1 and S2, Supporting Information, for a summary of all TGA and DSC values obtained).

3.4. Mechanical Behavior of LCEs

Uniaxial tensile testing was used to analyze the mechanical properties of the unmodified elastomers (E3, E4, and E6) and liquid crystal elastomers at the γ-position

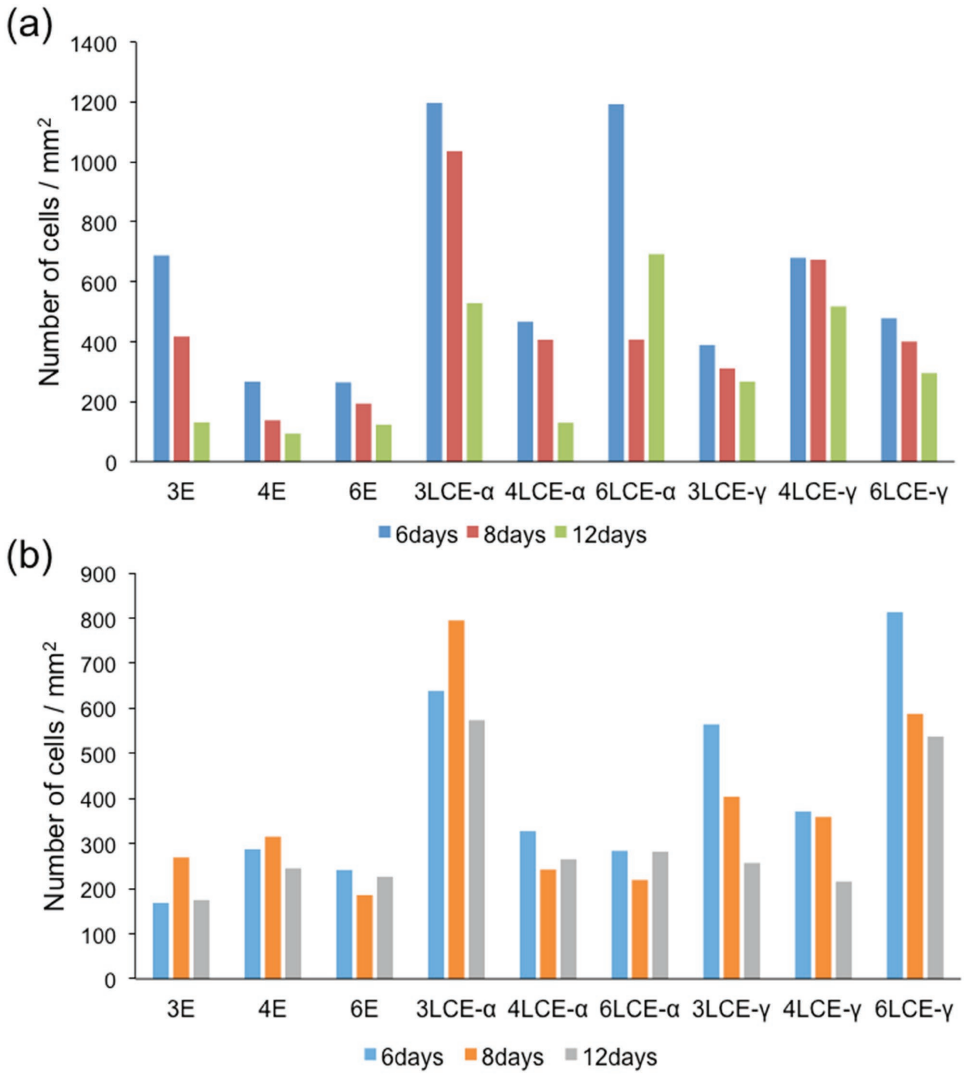

Figure 7. Cell viability assay using CyQuant for a) 1.5×10^4 C2C12 cells growing on (10 mm², rectangle 5 mm by 2 mm): unmodified, α-series LCEs and γ-series LCEs and b) 1.5×10^4 hDF cells growing on (10 mm², rectangle 5 mm by 2 mm): unmodified, α-series LCEs and γ-series LCEs.

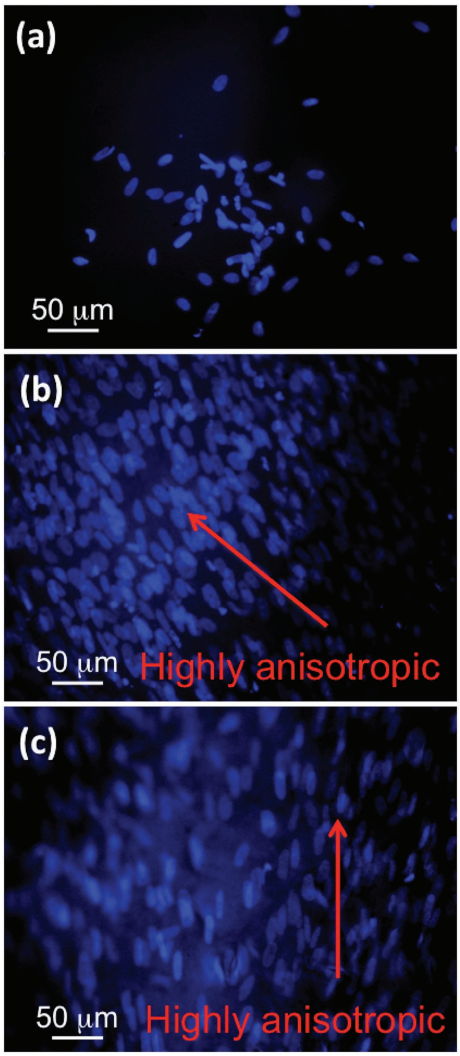

Figure 8. Primary human dermal fibroblast (hDF) cultures grown for 5 d on a) 3LCE-α, b) 4LCE-α, and c) 6LCE-α elastomer films.

(3LCE-γ, 4LCE-γ, and 6LCE-γ). Based on the representative stress–strain curves (Figure 5a) and calculated E values (Figure 5b), no clear correlations or trends were observed between the number of arms or the presence of LC pendant groups in the LCE films. Mechanical evaluation of the 4LCE-γ shows that modulus can potentially be affected due to the number of arms, which may correlate well with observations made during the cell culture experiments.[50,51] Previous theoretical and experimental studies have shown that tetra-arm polymer hydrogel systems have extremely high homogeneous packing and suppressed heterogeneity, which may explain the higher stiffness in 4LCE-γ and serving as a subject of future investigation.[52] We previously reported 3LCE-α and 3LCE-γ;[37] however, due to the new film preparation method the obtained 4LCE-α and 6LCE-α were weaker and broke more easily than their γ-counterparts (similar mechanical weakness was also observed during SAXD measurements). It is important to note that the moduli of all elastomers examined here are lower (≈2.0–4.0 MPa) than those of the tissues formed by the cells investigated (30 MPa for skin and 350 MPa for muscle) as well as lower than for other widely used biodegradable polymers, likely due to the low molecular weight and nonlinear star-block structure.[41,51,53] The mechanical properties obtained from the tensile stress–strain curves are summarized in Table S3 (Supporting Information). These preliminary mechanical results show a promising future for the use of LCEs in designing biomaterials for extracellular matrices. Cells are not only able to expand and proliferate, but tend to align on and within such LCE scaffolds without the use of any external stimuli.

3.5. Cell Studies

To determine the viability of cells on and within the LCEs we first tested murine myoblasts C2C12 cells on the α- and γ-series LCEs and for comparison also on the unmodified elastomers 3E to 6E. Figure 6 shows the fluorescence confocal images of cells cultured for 8 d on 3LCE-α, 4LCE-α, and 6LCE-α as well as on the unmodified elastomers. From these images, it can be seen that the α-series LCEs provide a better platform for the attachment and proliferation of C2C12 and hDF cells than the unmodified elastomers (indicated by a much higher number of much more evenly and closely spaced cell nuclei). This is further confirmed by the CyQuant cell viability assay. Figure 7a,b shows the CyQuant cell viability assays for both C2C12 and hDF growing on unmodified as well as the α- and γ-series LCEs. Both α- and γ-LCEs in general outperform their respective unmodified elastomer counterparts with the same central node by showing an overall increase in cell proliferation. We also observed that among all LCE-αs 3-arm LCEα showed a higher proliferation of both C2C12s and hDF cells. However, among the LCE-γ's, the 4LCE-γ showed the best proliferation rate for C2C12 cells while the 6LCE-γ was optimal for hDF cell proliferation. Since different cell types prefer an elasticity regime of the supporting scaffold matching native tissue,[41] we assume that the elastic properties, depending on the type and density of cross-linking

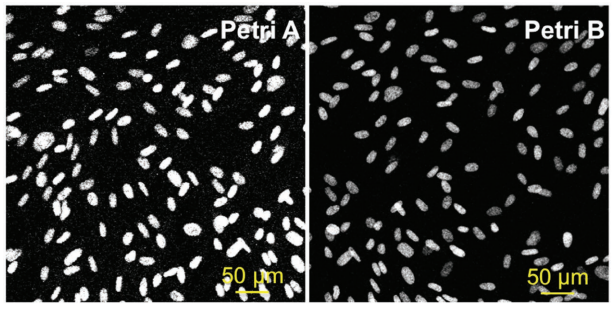

Figure 9. Directionality analysis of primary human dermal fibroblast (hDF) cells grown on petri dishes.

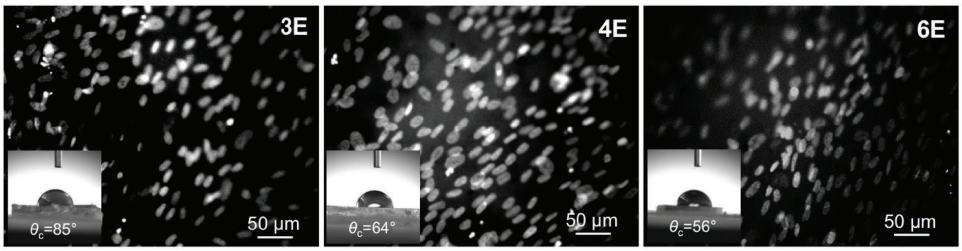

Figure 10. Directionality analysis of primary human dermal fibroblast (hDF) cells grown on: a) 3E, b) 4E, and c) 6E unmodified elastomers. The insets in each of the images show a photoimage and value from contact angle measurements.

imparted by the various central nodes, are responsible for this observation (especially considering that most other parameters are constant among each series). This highlights the fact that modified LCE's for cellular growth should be carefully selected based on the intended cell types to be grown to provide the most optimal proliferation rates. We also performed confocal microscopy studies of the α-series LCEs with primary hDF cells. Figure 8 shows the confocal fluorescence microscopy images of hDF cells cultured on the α-series LCEs for 5 d. Cell attachment, and by virtue of the cell number seeded on day 1, also proliferation, is seen on all three LCE scaffolds (3LCE-α, 4LCE-α, and 6LCE-α). Remarkable, however, is the fact that the images show anisotropic cell growth, especially for 4LCE-α and 6LCE-α. No external stimulus (i.e., stretching) was applied to the elastomer samples, indicating that directional cell growth might be a response to the lamellar (layer-like) molecular structure of the LC components (pendants) embedded within the scaffold network. However, additional and more detailed experiments on cell proliferation in the presence and absence of external stresses are required to gain further insight into this behavior. These studies are underway and will be reported at a later stage.

3.6. Cell Alignment Studies

The fluorescence confocal images and the directional growth analysis histograms of the hDF nuclei are shown and summarized in Figures 9–12 and Table S4 (Supporting Information). The directional analysis histograms of the hDF nuclei growing on commercially available petri dishes are summarized in Figure 8. Figure 8 suggests that elongated hDFs are aligned naturally in dense conditions such as almost 100% confluency. All petri dishes showed similar confluence. The dispersion ranges in petri dishes were between 7° and 24°. As seen in Figure 9 cells on petri dishes, however, show multi maxima in the directionality histograms (multimodal directional distribution), but overall the histograms suggest that cells could potentially grow with a common orientation in some locations of a petri dish.

The directional analysis histograms for the all elastomers are shown in Figure S16 (for 4LCE-γ at 8 d) and S17 (Supporting Information) (Summary of all directionality histograms of hDF cells grown on elastomers). The hDF cells grew randomly on 3E and 4E. On the other hand, the histogram of 6E shows a somewhat narrower distribution. It suggests that 6E can potentially allow cells to orient within a few locations on the elastomer. Overall, however, there little difference between cells growing on petri dishes and the unmodified elastomers.

Analyzing the cells growth on 3LCE-α (Figure 11a) also shows that cell orientation is virtually random, similar to the histograms obtained from analyzing images for cell attachment on petri dishes and the unmodified elastomers. In contrast, and highly noteworthy, the histograms of 4LCE-α and 6LCE-α show that cell attachment and growth are highly anisotropic, with 4LCE-α permitting the highest unimodal cell orientation of hDFs (Figure 10b,c). hDF cells on the 3LCE-γ, 4LCE-γ, and 6LCE-γ also show a narrow orientational dispersion of cells (Figure 12). In comparison, cell orientation on the γ-series LCEs was less uniform in comparison to the α-series LCEs. We assume

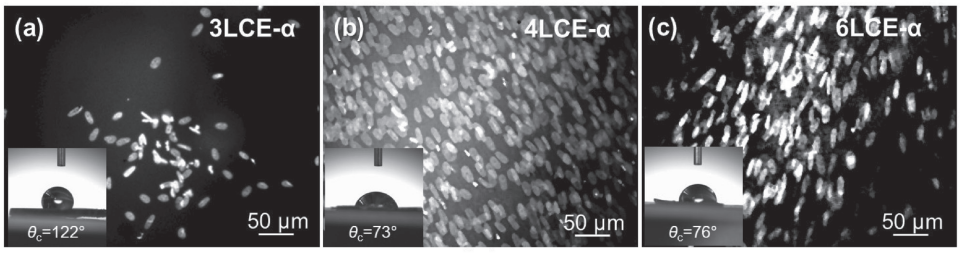

Figure 11. Directionality analysis of primary human dermal fibroblast (hDF) cells grown on a) 3LCE-α, b) 4LCE-α, and c) 6LCE-α elastomer films. The insets in each of the images show a photoimage and value from contact angle measurements.

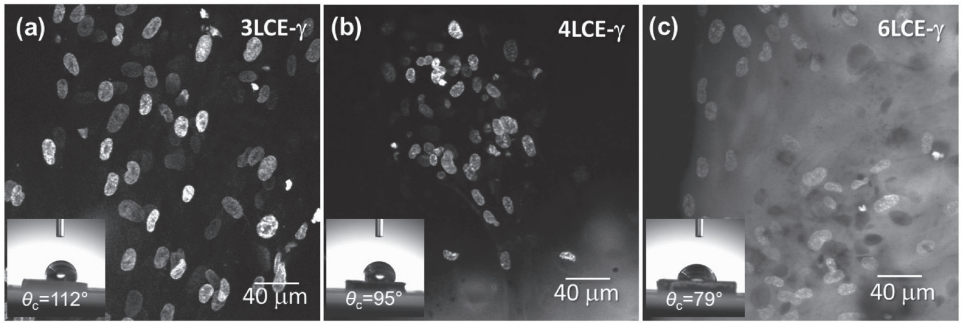

Figure 12. Directionality analysis of primary human dermal fibroblast (hDF) cells grown on a) 3LCE-γ, b) 4LCE-γ, and c) 6LCE-γ elastomer films. The insets in each of the images show a photoimage and value from contact angle measurements.

that the mechanical properties and the elevated hydrophobicity due to the more flexible LC pendants may contribute to a higher number of cholesterol pendants exposed on the surface of the synthesized γ-series LCEs. Particularly, 4LCE-γ and 6LCE-γ show higher contact angle values than the corresponding 4LCE-α and 6LCE-α, which could potentially inhibit cell growth at the same rate as on the α-series LCEs. Eventually, cells will continue to grow and proliferate but at a lower pace as shown in Figure S16 (Supporting Information) for hDF cells growing on 4LCE-γ imaged after 8 d.

4. Conclusions

We here presented the synthesis, characterization, mechanical, as well as, cell viability studies on smectic-A biocompatible, biodegradable, and porous cholesterol-based LCEs. In particular, 3-, 4-, and 6-arm (using glycerol, pentaerythritol, or dipentaerythritol) central nodes were investigated as initiators for obtaining star block-copolymers with cholesterol LC molecules as pendant groups within the polymer network. These polymers were further cross-linked to obtain elastomers with cholesterol LC pendants in α- or γ-position to the ε-CL carbonyl group. The type of central node and the position of cholesterol pendants in the backbone of the random ε-CL blocks both affect the overall morphology, the mechanical properties as well as cell proliferation and particularly cell alignment. Mechanical tests showed the highest stiffness for 4LCE-γ, but otherwise no notable difference between the 3- and 6-arm LCEs. These finding support the cell studies, where particularly 4LCE-γ showed the least tendency of cell alignment when compared to both 3LCE-γ and 6LCE-γ, which are both softer. Overall, our data clearly demonstrate that further studies are needed to gain a deeper understanding of the interplay between morphological as well as mechanical properties of elastomer-based scaffolds and cell attachment/alignment. Our preliminary mechanical studies indicate that 4LCE-γ shows an E tensile value of 4.0 MPa, which is reasonably close to the value reported by McKee et al.[41] for skin tissue (30 MPa), but much lower, however, than the value for muscle tissue (≈350 MPa), which perhaps explains why hDF cell cultures showed more pronounced alignment than the C2C12 cells on our LCE scaffolds. Future studies will now focus on modifying the elastomer structure to adjust the mechanical properties (both indentation and tensile) closer to particular tissues. Particularly promising could perhaps be large-scale modeling studies of such complex systems. Current, ongoing experiments in our laboratories are focusing on studying changes in ordering of the reported LCE scaffolds by applying mechanical stress with the aid of combined tensile-SAXD experiments and the cellular response to mechanical stress when embedded in the LCE scaffold.

Supporting Information

Supporting Information is available from the Wiley Online Library or from the author.

Acknowledgements: T.M., C.J.M., and H.R.E. contributed equally to this work. A.S., T.M., and E.H. drafted the article with contribution from other authors. A.S. performed most synthesis, characterization, and testing of materials, C.J.M. and H.R.E. assisted with the synthesis of key intermediates, helped with characterization and cell culture. T.M. with assistance from A.D.N. and Jessica Krieger performed cell studies; with assistance of C.J.M. and R.J.C. performed all cell viability tests and confocal fluorescence microscopy studies. L.L. assisted with POM measurements and cell cultures. M.T.L. did the mechanical testing. The authors want to thank Alex M. Jordan and Symone L. M. Alexander for their help with SAXD measurements for unmodified elastomer samples at the Argonne National Laboratory. The authors also thank Alex M. Jordan for help with contact angle measurements at the Department of Macromolecular Science and Engineering, Case Western Reserve University, Cleveland (Ohio). The authors are thankful to Dr. C. Zhu and Dr. E. Schaible for help with SAXD measurements at Advanced Light Source, Berkeley. The authors would like to thank dedicated undergraduates students Blake Kinsel, Sierra Crotty, Brandy Marks and Richard Cukelj who helped with the synthesis and cell culture. The authors would like to thank the

U.S. National Science Foundation (NSF) for financial support (CHE-1263087). T.H. greatly appreciates financial support from the Ohio Third Frontier (OTF) Program for Ohio Research Scholars "Research Cluster on Surfaces in Advanced Materials", which also supports the Materials Characterization facility at Liquid Crystal Institute (LCI), where current SEM images were obtained. This research used resources of the Advanced Photon Source, a U.S. Department of Energy (DOE) Office of Science User Facility operated for the DOE Office of Science by Argonne National Laboratory under Contract No. DE-AC02-06CH11357. Beamline 7.3.3 of the Advanced Light Source is supported by the Director of the Office of Science, Office of Basic Energy Sciences, of the U.S. Department of Energy under Contract No. DE-AC02-05CH11231. The authors declare no competing financial interest.

This article was modified on February 16, 2017 to optimize Scheme 1.

Received: July 6, 2016; Revised: September 23, 2016; Published online: November 2, 2016; DOI: 10.1002/mabi.201600278

Keywords: 3D porous scaffolds; cell alignment; cell directionality; liquid crystal elastomers; mechanics

[1] R. P. Mecham, P. D. Yurchenco, D. E. Birk, *Extracellular Matrix Assembly and Structure*, San Diego, Academic Press **1994**.
[2] J. K. Kular, S. Basu, R. I. Sharma, *J. Tissue Eng.* **2014**, *5*, 1.
[3] R. Langer, D. A. Tirrell, *Nature* **2004**, *428*, 487.
[4] M. P. Lutolf, J. A. Hubbell, *Nat. Biotechnol.* **2005**, *23*, 47.
[5] E. S. Place, N. D. Evans, M. M. Stevens, *Nat. Mater.* **2009**, *8*, 457.
[6] K. Kyburz, K. Anseth, *Ann. Biomed. Eng.* **2015**, *43*, 489.
[7] J. Rnjak-Kovacina, L. S. Wray, K. A. Burke, T. Torregrosa, J. M. Golinski, W. Huang, D. L. Kaplan, *ACS Biomater. Sci. Eng.* **2015**, *1*, 260.
[8] A. Lendlein, R. Langer, *Science* **2002**, *296*, 1673.
[9] A. G. A. Coombes, S. C. Rizzi, M. Williamson, J. E. Barralet, S. Downes, W. A. Wallace, *Biomaterials* **2004**, *25*, 315.
[10] P. Y. W. Dankers, M. C. Harmsen, L. A. Brouwer, Van Luyn, J. A. Marja, E. W. Meijer, *Nat. Mater.* **2005**, *4*, 568.
[11] A. Atala, S. B. Bauer, S. Soker, J. J. Yoo, A. B. Retik. *Lancet* **2006**, *367*, 1241.
[12] N. Rapoport, *Prog. Polym. Sci.* **2007**, *32*, 962.
[13] D. F. Williams, *Biomaterials* **2008**, *29*, 2941.
[14] W. Zimmermann, *Nat. Mater.* **2008**, *7*, 932.
[15] C. Lou, C. Yao, Y. Chen, T. Hsieh, J. Lin, W. Hsing, *Text. Res. J.* **2008**, *78*, 958.
[16] C. Byrne, T. Church, J. Kramer, G. Coates. *Angew. Chem., Int. Ed.* **2008**, *47*, 3979.
[17] E. Yuksel, *Semin. Plast. Surg.* **2005**, *19*, 261.
[18] R. J. Pelham, Y. Wang, *Proc. Natl. Acad. Sci. USA* **1997**, *94*, 13661.
[19] A. J. Engler, S. Sen, H. L. Sweeney, D. E. Discher, *Cell* **2006**, *126*, 677.
[20] W. Li, R. L. Mauck, J. A. Cooper, X. Yuan, R. S. Tuan, *J. Biomech.* **2007**, *40*, 1686.
[21] L. E. Millon, H. Mohammadi, W. K. Wan, *J. Biomed. Mater. Res., Part B* **2006**, *79*, 305.
[22] B. Sun, X. Jiang, S. Zhang, J. Zhang, Y. Li, Q. You, Y. Long, *J. Mater. Chem. B* **2015**, *3*, 5389.
[23] G. C. Engelmayr, M. Cheng, C. J. Bettinger, J. T. Borenstein, R. Langer, L. E. Freed, *Nat. Mater.* **2008**, *7*, 1003.
[24] E. Cukierman, R. Pankov, D. R. Stevens, K. M. Yamada, *Science* **2001**, *294*, 1708.
[25] M. M. Stevens, J. H. George, *Science* **2005**, *310*, 1135.
[26] S. J. Hollister, *Nat. Mater.* **2005**, *4*, 518.
[27] A. W. Orr, B. P. Helmke, B. R. Blackman, M. A. Schwartz. *Dev. Cell* **2006**, *10*, 11.
[28] F. T. Moutos, L. E. Freed, F. Guilak, *Nat. Mater.* **2007**, *6*, 162.
[29] A. M. Lowe, N. L. Abbott, *Chem. Mater.* **2012**, *24*, 746.
[30] H. R. Brand, H. Finkelmann, D. Demus, J. Goodby, G. W. Gray, H. Spiess, V. Vill, *Handbook of Liquid Crystals, Volume 3, High Molecular Weight Liquid Crystals*, Wiley-VCH Verlag GmbH 1998, **2008**, p. 277.
[31] P. De Gennes, M. Hébert, R. Kant, *Macromol. Symp.* **1997**, *113*, 39.
[32] H. Finkelmann, S. T. Kim, A. Muñoz, P. Palffy-Muhoray, B. Taheri, *Adv. Mater.* **2001**, *13*, 1069.
[33] M. Camacho-Lopez, H. Finkelmann, P. Palffy-Muhoray, M. Shelley, *Nat. Mater.* **2004**, *3*, 307.
[34] Y. Yu, T. Ikeda. *Angew. Chem., Int. Ed.* **2006**, *45*, 5416.
[35] C. L. van Oosten, C. W. M. Bastiaansen, D. J. Broer, *Nat. Mater.* **2009**, *8*, 677.
[36] N. A. Lockwood, J. C. Mohr, L. Ji, C. J. Murphy, S. P. Palecek, J. J. de Pablo, N. L. Abbott, *Adv. Funct. Mater.* **2006**, *16*, 618.
[37] A. Sharma, A. Neshat, C. J. Mahnen, A. d. Nielsen, J. Snyder, T. L. Stankovich, B. G. Daum, E. M. LaSpina, G. Beltrano, Y. Gao, S. Li, B. Park, R. J. Clements, E. J. Freeman, C. Malcuit, J. A. McDonough, L. T. J. Korley, T. Hegmann, E. Hegmann, *Macromol. Biosci.* **2015**, *15*, 200.
[38] Y. Gao, T. Mori, S. Manning, Y. Zhao, A. d. Nielsen, A. Neshat, A. Sharma, C. J. Mahnen, H. R. Everson, S. Crotty, R. J. Clements, C. Malcuit, E. Hegmann, *ACS Macro Lett.* **2016**, *5*, 4.
[39] T. Bera, E. J. Freeman, J. A. McDonough, R. J. Clements, A. Aladlaan, D. W. Miller, C. Malcuit, T. Hegmann, E. Hegmann, *ACS Appl. Mater. Interfaces* **2015**, *7*, 14528.
[40] T. Bera, C. Malcuit, R. J. Clements, E. Hegmann, *Front. Matter* **2016**, *3*, 31.
[41] C. T. McKee, J. A. Last, P. Russell, C. J. Murphy, *Tissue Eng., Part B* **2011**, *17*, 155.
[42] J. S. Dahl, C. E. Dahl, *Proc. Natl. Acad. Sci. USA* **1983**, *80*, 692.
[43] D. H. Mauch, K. Nägler, S. Schumacher, C. Göritz, E. Müller, A. Otto, F. W. Pfrieger, *Science* **2001**, *294*, 1354.
[44] J. J. Hwang, S. N. Iyer, L. Li, R. Claussen, D. A. Harrington, S. I. Stupp, *Proc. Natl. Acad. Sci. USA* **2002**, *99*, 9662.
[45] K. Nagahama, Y. Ueda, T. Ouchi, Y. Ohya, *Biomacromolecules* **2007**, *8*, 3938.
[46] A. Hexemer, W. Bras, J. Glossinger, E. Schaible, E. Gann, R. Kirian, A. MacDowell, M. Church, B. Rude, H. Padmore, *J. Phys.: Conf. Ser.* **2010**, *247*, 012007.
[47] C. A. Schneider, W. S. Rasband, K. W. Eliceiri, *Nat. Methods* **2012**, *9*, 671.
[48] H. M. Younes, E. Bravo-Grimaldo, B. G. Amsden, *Biomaterials* **2004**, *25*, 5261.
[49] W. H. Binder, R. Sachsenhofer. *Macromol. Rapid Commun.* **2008**, *29*, 952.
[50] B. D. Ratner, S. J. Bryant, *Annu. Rev. Biomed. Eng.* **2004**, *6*, 41.
[51] I. Armentano, M. Dottori, E. Fortunati, S. Mattioli, J. M. Kenny, *Polym. Degrad. Stab.* **2010**, *95*, 2126.
[52] T. Sakai, *Polym. J.* **2014**, *46*, 517.
[53] L. S. Nair, C. T. Laurencin, *Prog. Polym. Sci.* **2007**, *32*, 762.